Journal of
Vascular Surgery
Venous and Lymphatic Disorders™

# Hemodynamic coupling of a pair of venous valves

Wei-Hsin Tien, PhD,[a] Henry Y. Chen, PhD,[b,d,e] Zachary C. Berwick, PhD,[b,d] Joshua Krieger, BSME,[f] Sean Chambers, PhD,[f] Dana Dabiri, PhD,[a] and Ghassan S. Kassab, PhD,[c,d,e] *Seattle, Wash; and Indianapolis and Bloomington, Ind*

***Background:*** **In vivo studies have shown that valves in veins are paired in an orthogonal configuration. The aim of this study is to characterize the flow interaction of paired valves under controlled in vitro bench conditions.**

***Methods:*** **A bench top in vitro experiment was set up at physiological flow conditions to simulate the flow inside a venous valve. Two bicuspid bioprosthetic valves paired in 0° and 90° orientations were tested in a 12-mm-diameter tube, and the two-dimensional velocity fields around the valve were measured by particle image velocimetry. The distance between the two valves was varied from 3 to 5 cm, and the corresponding velocities and vorticities were determined.**

***Results:*** **Velocity field shows the flow exit from the orthogonal valve-pairing configurations forced the main jet stream to turn to the outer region of the tube. Flow patterns between the valves show significantly less stagnation region from the 90° valve pairing over a 0° valve pairing case. The variation in valves distance shows that the coupling effect of the two valves extends to a range beyond four times of the tube diameter, albeit the ability to alter the flow decreases at larger distances.**

***Conclusions:*** **The findings suggest that the 90° valve pairing configuration regulates the flow between the valves, and the separation distance affects the hemodynamic efficiency of the two valves by reducing the total reverse flow volume. (J Vasc Surg: Venous and Lym Dis 2014;■:1-12.)**

***Clinical Relevance:*** **This experimental work investigates the functions and performance of bioprosthetic venous valves coupled in orthogonal configurations. The effect of coupled venous valves was shown to be a determining factor in creating a more natural, helical flow pattern, which helps to optimize venous return. The results of this study provide valuable information that will improve not only the current understanding of blood flow patterns around native venous valves, but also the design of future prosthetic valves. Better prosthetic valve designs based on this work will provide a more effective alternative treatment for chronic venous insufficiency.**

Venous valves play a central role in the blood circulation of the lower extremities. Dysfunction of venous valves is the main cause of chronic venous inefficiency. Valve incompetence results in venous reflux and distal venous hypertension, which can lead to venous remodeling, inflammation, and prothrombotic changes of the endothelium.[1,2] Although the basic function of valves has been realized for many years, it is not until recently that advances in imaging have revealed interesting details about the venous valve. Animal and human studies show that the valve does not fully open[3,4] but forms a pocket region with the sinus wall to create a vortex structure behind the valve leaflets. A study by Lurie et al[5] showed that four phases can be identified in a complete valve cycle. Complex fluid mechanics phenomenon, such as flow separation and reattachment, and vortical flow in the sinus are likely to play important roles in the operation of the valves. The valve is also a modulator of the venous flow in addition to preventing retrograde flow in the vein. Nam et al[6] applied the velocimetry technique to veins with a high-frequency ultrasound image system to image the flow around the perivalvular area in a human superficial vein. Using echo speckles of red blood cells as flow tracers, the motions of valve cusps were simultaneously visualized, and large-scale vortices were observed behind the sinus pocket while the main bloodstream was directed proximally.

Although the functionality of a single venous valve has been studied, less attention has focused on the coupling effect of multiple valves. Anatomy of the lower extremity veins shows that the distribution of the valves is not uniformly spaced in the venous system. For example, in the great saphenous vein, there are more valves located below than above the knee. Similarly, there are more valves in the tibial veins than popliteal veins and femoral.[7] Studies show that despite individual variability at the saphenofemoral junctions, multiple valves are present and the distance between two valves is approximately 3 to 5 cm.[1,8-10] These observations suggest that where and how the valves are spaced is important for the performance of the venous system.

Recently, Lurie and Kistner[11] studied 15 healthy volunteers and 13 unaffected limbs of patients with unilateral

From the Department of Aeronautics and Astronautics, University of Washington, Seattle[a]; the Research and Development, 3DT Holdings, LLC, Indianapolis[b]; the Departments of Surgery[c] and Cellular and Integrative Physiology,[d] Indiana University School of Medicine, Indianapolis; the Department of Biomedical Engineering, Indiana University Purdue University Indianapolis, Indianapolis[e]; and Research Engineering, Cook Medical, Bloomington.[f]

This research was supported by 3DT Holdings, LLC and Cook Medical.

Author conflict of interest: The prosthetic valves used in this study are designed and manufactured by Cook Medical Inc. Dr Kassab is the founder of 3DT. Mr Chambers and Mr Krieger are employees of Cook Medical Inc.

Reprint requests: Ghassan S. Kassab, PhD, Department of Biomedical Engineering, Indiana University Purdue University Indianapolis, 635 Barnhill Dr, Indianapolis, IN 46202 (e-mail: gkassab@iupui.edu).

The editors and reviewers of this article have no relevant financial relationships to disclose per the Journal policy that requires reviewers to decline review of any manuscript for which they may have a conflict of interest.

2213-333X/$36.00



http://dx.doi.org/10.1016/j.jvsv.2013.09.008

primary chronic venous disease. The distance and relative position between the two most proximal valves of the great saphenous vein and femoral vein were identified. The mean distance was found to be 3.8 to 4.6 cm, and the mean angle between the valve orientations was 84° to 88°. They hypothesized that this valve configuration increases the efficiency of venous return by creating a helical three-dimensional (3D) flow pattern. This was confirmed by a more recent study[12] using color and spectral Doppler imaging to calculate the velocity vectors at five cross-sectional planes of femoral and common femoral veins. Helical flow was present in close proximity and downstream from a valve and at valve junction, and was more prevalent when the calf muscle pump was active. When the valve was incompetent, the helical flow pattern disappeared and was replaced by disorganized flow. Helical flow patterns have been studied extensively in the heart and arterial systems,[13-15] and it was found that the helical flow limits flow instability[16,17] and increases the efficiency of the flow system.[18] These findings suggest that the venous valves may play a similar role to improve the efficiency and stabilize the blood flow in the venous system.

The previous studies were done in vivo and provide qualitative observations on flow patterns around a pair of valves. Due to the technological limitations, however, quantitative analysis of the flow field was limited to the bulk velocity, and the detailed velocity distribution was unattainable. Since all of the valve pairs observed in the previous in vivo studies were misaligned by at least 60°, no control group (0° alignment) was investigated in vivo to study the coupling effect between the valves. The objective of this study is to overcome some of these limitations by the use of a high-resolution particle imaging velocimetry (PIV) technique to study the flow around a pair of prosthetic venous valves (at various angles and separation distances) in an in vitro setup. The PIV technique provides higher-resolution velocity distribution around the valve and the temporal evolution of the flow pattern of each valve phase as compared to in vivo ultrasound. A control group with a valve pair of 0° apart was tested, and distance between the valve pair was varied to investigate the coupling effect of valves. The results provide a more detailed understanding of the flow pattern around the venous valve and complement the in vivo observations.

## METHODS

A pulse duplicator (PD) was utilized (BDC Laboratories, Wheat Ridge, Colo) to generate pulsatile flow through a venous valve with a bench top flow loop. Physiologic pressures and flow were duplicated and recorded for subsequent analysis. The flow system provided flow directional control and mean pressure control.

The test section consisted of a square container made of Plexiglas and a round glass tube (12 mm ID) to mimic the geometry of the vein. Two pressure transducers were used to measure the upstream and downstream pressure of the test section to evaluate the valve performance. An ultrasound flow probe (ME13PXN; Transonic System Inc, Ithaca, NY) was mounted upstream to provide flow rate measurement of the system. For experiments in the present study, the mean flow rate was set at 0.35 L/min at 15 beats per minutes rate, and the peak pressure difference under diastolic phase was adjusted to 2 mm Hg. The pressure and flow rate data were recorded at a 5-kHz data rate for 15 seconds, and the data were phase-averaged after processing.

The bioprosthetic valves used for the present study were provided by Cook Biotech Inc (West Lafayette, Ind). The bicuspid valves were the third-generation bioprosthetic venous valve frame with a 12-mm nominal diameter; detailed information of the valve can be found in Pavcnik et al.[19] The proximal side and distal side refer to the leaflet surfaces that were facing the venous flow proximal or distal to the heart.

To mimic the viscosity of blood and reduce the image distortion because of refraction, the working fluid was a solution of glycerol and water at a volume ratio of 2:3 with a resultant viscosity of 3.6 cP (25°C) with a 1.4 refraction index. At the current testing conditions, the Reynolds and Womersley numbers were 358 and 4.5, respectively.

PIV setup was used in conjunction with the PD flow loop platform to perform the velocity measurements. A double-pulsed Nd:YAG laser (Solo 120XT; New Wave Research, Fremont, Calif) was used to illuminate the flow tracers. The PD flow loop was seeded with polystyrene fluorescent particles (Nile Red 10-14 μm; Spherotech, Lake Forest, Ill). The fluorescent lights emitted from the particles were excited by the 532-nm wavelength illuminating laser light. Lens optics was used to shape the laser beam into a thin laser sheet ($\sim$1 mm) to illuminate the area of interest. A 10-bit monochrome CCD camera (UP-1830-10; Uniq Vision, Santa Clara, Calif) was used to capture tracer motions within this area. The resolution of the camera was 1024 × 1030 pixels to provide a 15.4-μm/pixel spatial resolution, corresponding to an imaging area of 15.8 × 15.9 mm.

The PIV images were first preprocessed to remove the valve area and reflections from the glass wall. The interrogation window used in the PIV processing algorithm was set with a 50% overlap and iteratively refined to 48 × 48 pixels with the window deformation technique.[20] Vector outliers were identified using the universal outlier detection method[21] and then replaced by interpolating the neighboring vectors.

Fig 1 shows the coordinate system used in the experiments and the PIV measurement locations. The valve orientation was defined as the angle $\Theta$ to the horizontal plane (X-Z plane) in Fig 1. The angle between the two valves, $\Theta_2$-$\Theta_1$, was set to 0° and 90°. To investigate the coupling effect of the two valves, three different separation distances D = 3, 4, and 5 cm were tested. The nondimensionalized separation distances normalized by the tube diameter (d) were 2.5 d, 3.3 d, and 4.2 d, respectively. There were a total of six different valve pairing configurations tested, and the details are listed in Table I. The separation distance and angle between the valve pair in these configurations are chosen based on Lurie and Kistner's study.[11] The configurations with 0° pairing angle were added to further investigate the effect of the angle (valve

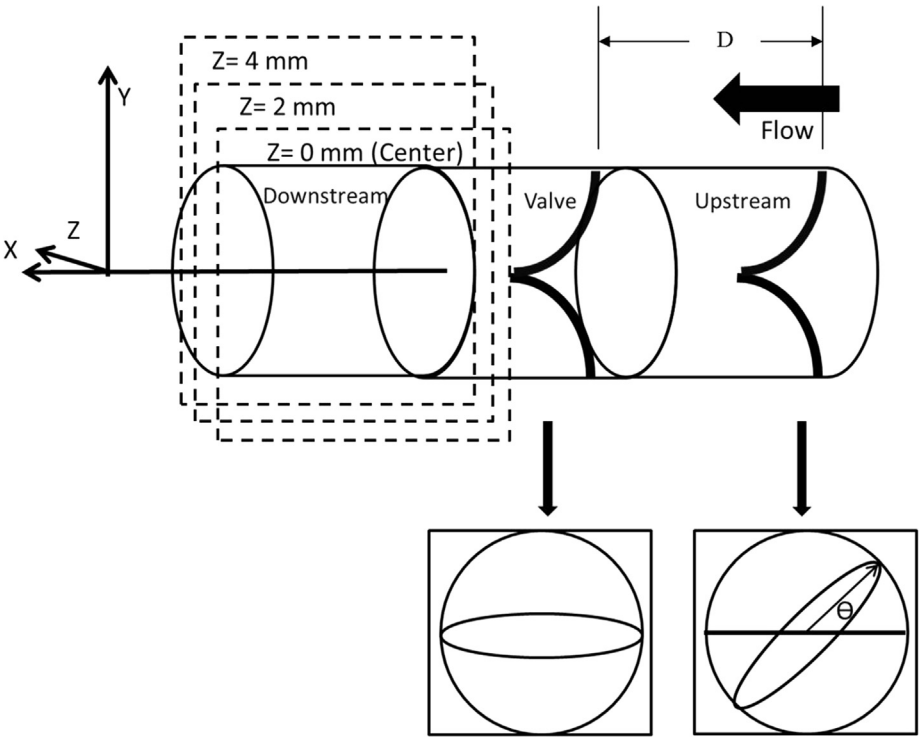


**Fig 1.** Coordinate system used in the study and the measurement locations.

**Table I.** Valve pairing configurations tested

| *Valve pairing configuration* | *Separating distance (D)* | $\theta_2 - \theta_1$ |
|---|---|---|
| 1 | 4 cm | 0° |
| 2 | 4 cm | 90° |
| 3 | 5 cm | 0° |
| 4 | 5 cm | 90° |
| 5 | 3 cm | 0° |
| 6 | 3 cm | 90° |

pairing 1, 3, and 5), since in the in vivo study the angle between the valve pair only spread from 60° to 100° in vivo.[11]

Based on conservation of mass principle that relates the gradients of the three velocity components, the two-dimensional (2D) velocity results show that the flow around the valve is 3D. The PIV technique used in the current study is 2D and only measures the velocity components in the in-plane direction (X and Y). Since the tube is circular and the bicuspid valve structure is not axisymmetric, it is possible to verify the three-dimensionality of the flow. This can be done by checking the mass conservation in the X and Y direction. Based on conservation of mass of incompressible flow, the flow is 2D if the flow rate across the tube is the same. Therefore, the velocity integral along the Y direction across the tube at different X locations can be used to verify the three dimensionality of the flow.

## RESULTS

### Hemodynamics

The flow data of a single valve are shown in Fig 2 where the four phases of the valve cycle defined by Lurie et al[5] were identified. The bulk flow rate increases with two different slopes until it reaches a peak value. This period is the opening phase and the equilibrium phase. The flow rate then decreases to a negative peak value and the pressure difference increases, and this period is the valve closing phase. The flow rate then stabilizes near zero until the end of the cycle, and the pressure difference starts to build up after the flow rate reaches the minimum magnitude. This period is the closed valve phase.

A single cycle of the pressure, and the difference between the upstream and downstream pressure, are shown in Figs 3 and 4, respectively for all valve pairing configurations, and the single-valve case are included for comparison. The pressure and flow data are very similar, except the smaller pressure difference of the single-valve case. This is as expected because the pressure drop is larger from the two valves. Table II shows the performance indices calculated from the pressure and flow data. The closing, leakage, and total reverse flow volume are calculated by integrating the flow curve through valve closing (ie, full closure phases). Most of the indices are similar for all six configurations, with the exception of total reverse flow volume shown in Fig 5. In all six cases, pairing configuration 2 (D = 3.3 d, 4 cm, $\Theta 2\text{-}\Theta 1 = 90°$) has the lowest

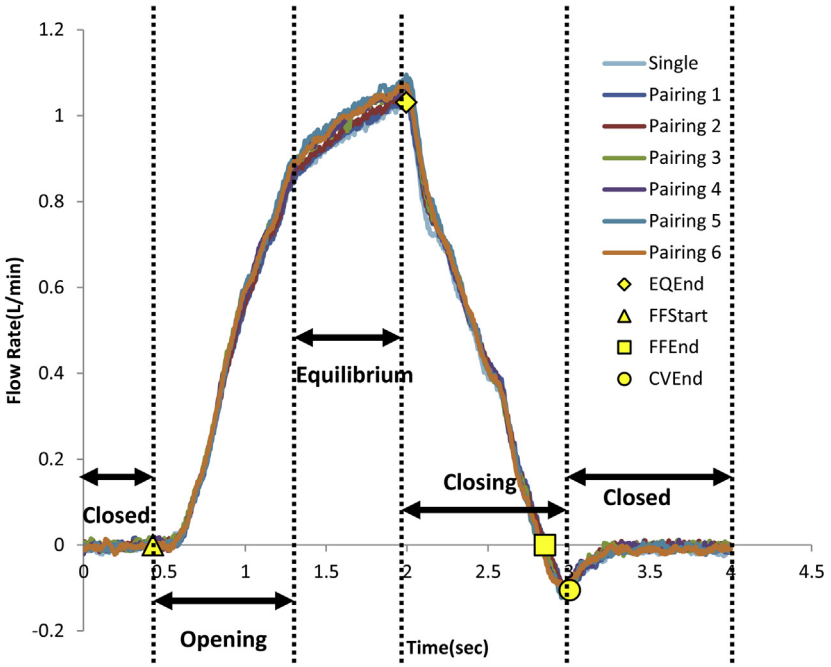


**Fig 2.** Flow rate of a valve cycle of all testing configurations in the present study. Start of forward flow (*FFStart*) and end of forward flow (*FFEnd*) are marked by the *yellow triangle* and *square*, respectively. End of equilibrium (*EQEnd*) is marked by the *yellow diamond*, and end of closing volume (*CVEnd*) is marked by the *yellow circle*. The four valve phases are identified and marked in the plots.

reverse flow volume. For the 0° configurations (valve pairing 1, 3, and 5), the total reverse flow volume increases with decreasing valve separation distance. For the 90° configurations (valve pairing 2, 4, and 6), the total reverse flow volume is smallest at D = 3.3 d (4 cm), and is largest at D = 2.5 d (3 cm).

## PIV measurements

**Effect of valve configuration.** Fig 6 shows the velocity fields downstream of the second valve overlaid with the calculated vorticity map at the center plane of the valve pairing 1, 2, and the single valve. During the equilibrium phase, a jet flow was formed at the valve exit where the flow reached maximum speed and the entrainment from the side is also at maximum. In the single-valve configuration, the flow was steady and the shear flow regions that have high vorticity on the jet boundaries were stable. This was not the case for the valve-pairing configurations. In both cases, the flow became unstable and the shear layer broke into vortex sheets. This is suggested by the concentrated regions of vorticity shown in Fig 6. The flow of the valve pairing 2 made a turn toward the upper wall at 0.3 d downstream of the valve exit. In the single-valve and valve pairing 1 case, the jet flow was straight and did not turn.

The influence of the valve-pairing configuration extends to further downstream of the flow. Fig 7 shows the downstream velocity fields overlaid with the velocity magnitude map in the equilibrium phase. In the single-valve case, the jet stream was strong and extended across the measurement plane with the ambient flow kept unchanged. In valve pairing 1, the jet only maintained a relatively short distance (~0.6 d) and then expanded to mix with the ambient fluid. In valve pairing 2, the jet flow was also mixed with the ambient fluid and expanded out similar to that in the valve pairing 1. The jet stream was also shifted off-center as valve pairing 1, and a strong vortex structure was formed at the center region. The vortex structure blocked the way and caused the jet stream to turn to the edge region of the tube.

The flow in between the two valves was altered the most by the various configurations. Fig 8 shows the comparison of the flow patterns in between the valves at equilibrium phase. The flow at Z = 0 (0 mm), Z = 0.17 d (2 mm) and Z = 0.35 d (4 mm) was measured, but only the center (Z = 0) and edge (Z = 0.17 d) planes are shown. The flow in valve pairing 1 shows the jet structure was shifted off-center, which was similar to the case shown in single-valve downstream in Fig 7. The jet flow structure coming out of the first valve remained unchanged until the inlet region of the second valve, and then it turned to the center region of the tube near the rear of the second valve. The jet flow region spread out as Z increased because the momentum is transported to the low-speed region. At the lower half of the tube, the flow was mostly stagnant with a small reverse flow region due to the shear flow at the edge of the jet stream. In valve pairing 2, the jet flow was uniform across the measurement plane (X-Y plane)

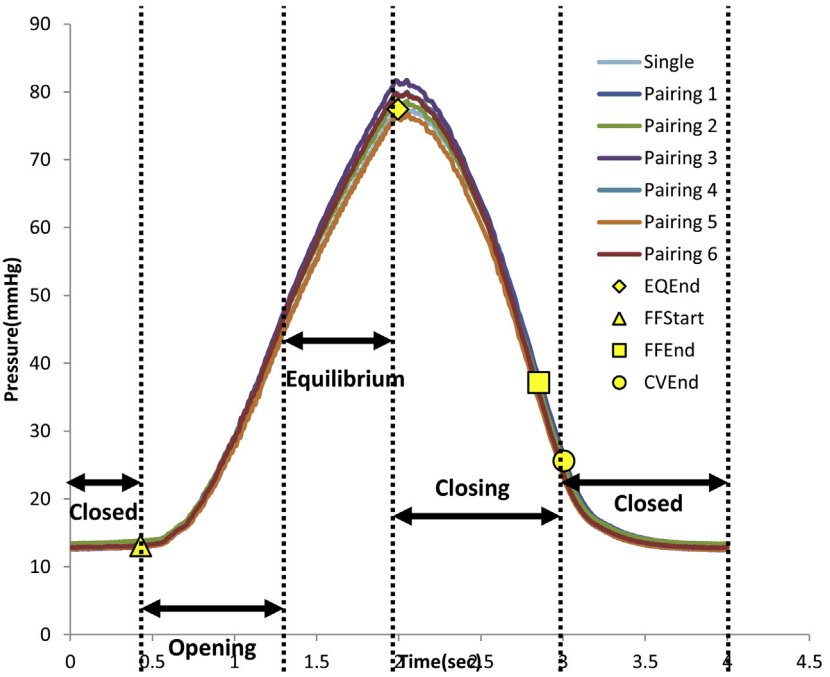


**Fig 3.** Valve inflow pressure of a valve cycle of all testing configurations in the present study. Start of forward flow (*FFStart*) and end of forward flow (*FFEnd*) are marked by a *yellow triangle* and *square*, respectively. End of equilibrium (*EQEnd*) is marked by the *yellow diamond*, and end of closing volume (*CVEnd*) is marked by the *yellow circle*. The four valve phases are identified and marked in the plots.

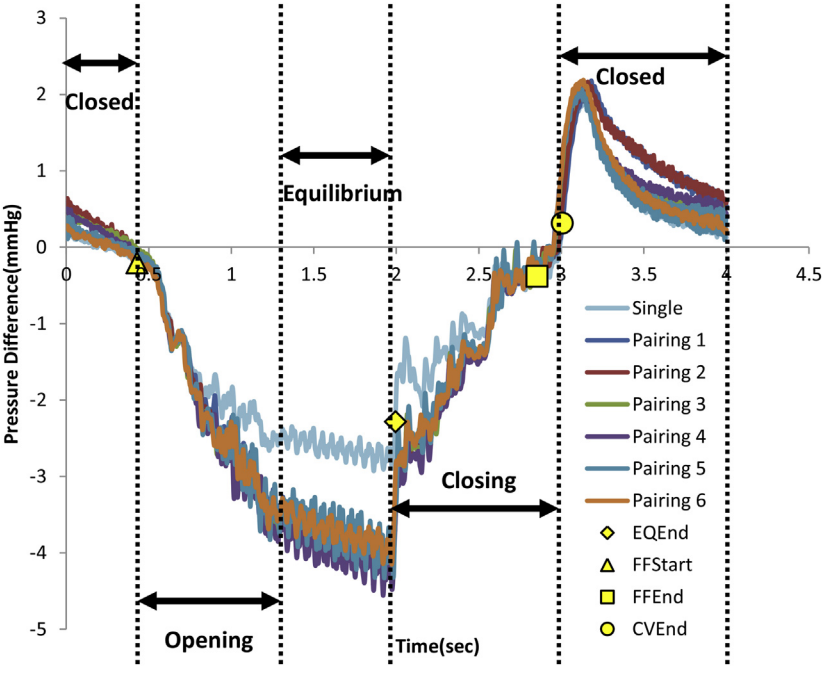


**Fig 4.** Pressure difference between inflow and outflow valve pressure of a valve cycle of all testing configurations in the present study. Start of forward flow (*FFStart*) and end of forward flow (*FFEnd*) are marked by a *yellow triangle* and *square*, respectively. End of equilibrium (*EQEnd*) is marked by the *yellow diamond*, and end of closing volume (*CVEnd*) is marked by the *yellow circle*. The four valve phases are identified and marked in the plots.

**Table II.** Hemodynamic indices of all the valve pairing configurations tested

| | *Single* | *Pairing 3 (5 cm, $\theta_2 - \theta_1 = 0°$)* | *Pairing 1 (4 cm, $\theta_2 - \theta_1 = 0°$)* | *Pairing 5 (3 cm, $\theta_2 - \theta_1 = 0°$)* | *Pairing 4 (5 cm, $\theta_2 - \theta_1 = 90°$)* | *Pairing 2 (4 cm, $\theta_2 - \theta_1 = 90°$)* | *Pairing 6 (3 cm, $\theta_2 - \theta_1 = 90°$)* |
|---|---|---|---|---|---|---|---|
| Closing volume, mL | −0.17 | −0.13 | −0.15 | −0.15 | −0.14 | −0.15 | −0.17 |
| Leakage volume, mL | −0.48 | −0.31 | −0.33 | −0.40 | −0.33 | −0.25 | −0.41 |
| Total regurgitate volume, mL/min | 9.8 | 6.6 | 7.2 | 8.2 | 7.0 | 6.0 | 8.7 |
| Stroke volume, mL | 24 | 24 | 24 | 24 | 24 | 24 | 24 |
| Mean regurgitate flow, mL/s | −0.43 | −0.28 | −0.30 | −0.34 | −0.29 | −0.25 | −0.37 |
| Regurgitate velocity | −2.4 | −1.9 | −2.0 | −2.2 | −1.9 | −1.7 | −2.4 |
| Percent closing volume time, % | 3.6 | 3.5 | 3.6 | 3.3 | 3.1 | 3.6 | 3.7 |
| Closing time for valve, seconds | 0.14 | 0.14 | 0.14 | 0.13 | 0.12 | 0.14 | 0.15 |
| Percent leakage volume time, % | 38 | 39 | 40 | 40 | 40 | 39 | 39 |
| Regurgitation fraction volume, % | −2.7 | −1.8 | −2.0 | −2.2 | −1.9 | −1.7 | −2.4 |
| Percent stroke volume time, % | 58 | 57 | 57 | 57 | 57 | 57 | 57 |
| Systolic duration, % | 62 | 61 | 60 | 60 | 60 | 61 | 61 |
| Peak positive pressure difference, mm Hg | −0.28 | −0.28 | −0.57 | −0.30 | −0.52 | −0.53 | −0.49 |
| Mean positive pressure difference, mm Hg | −2.2 | −3.1 | −3 | −2.9 | −3 | −3.1 | −3 |
| RMS forward flow, mL/s | 13 | 13 | 13 | 13 | 13 | 13 | 13 |
| Mean forward flow, mL/s | 10 | 11 | 10 | 11 | 11 | 10 | 11 |
| Effective orifice area, $cm^2$ | 0.18 | 0.15 | 0.15 | 0.16 | 0.15 | 0.15 | 0.15 |
| Cardiac output, mL/min | 370 | 371 | 360 | 371 | 369 | 364 | 372 |

The details of the pairing configurations are listed in Table I.

as seen from a top view of the valve. At Z = 0.35 d (4 mm), the velocity at the inner region was slower than the outer region. The stagnant region was smaller than that in the valve pairing 1, and no reverse flow was found.

**Effect of valve-separating distance.** Fig 9 shows the velocity vectors overlaid with a vorticity map at the equilibrium phase at the center plane for valve configuration 1-6. In all six cases, jet flows exited the valves inclined to the tube wall. The flow pattern is the most complex in the D = 2.5 d (3 cm) case, and several vortex-concentrated regions were formed at the shear layer. In the D = 3.3 d (4 cm) cases, the shear layer was more continuous and uniform. Valve pairing 2 had the most uniform vorticity distribution of the six cases. The vorticity patterns became more similar to each other for D = 4.2 d (5 cm) cases.

Fig 10 shows the velocity fields overlaid with the fluid shear calculated from the velocity data for all six configurations at different Z locations around the valve region. The

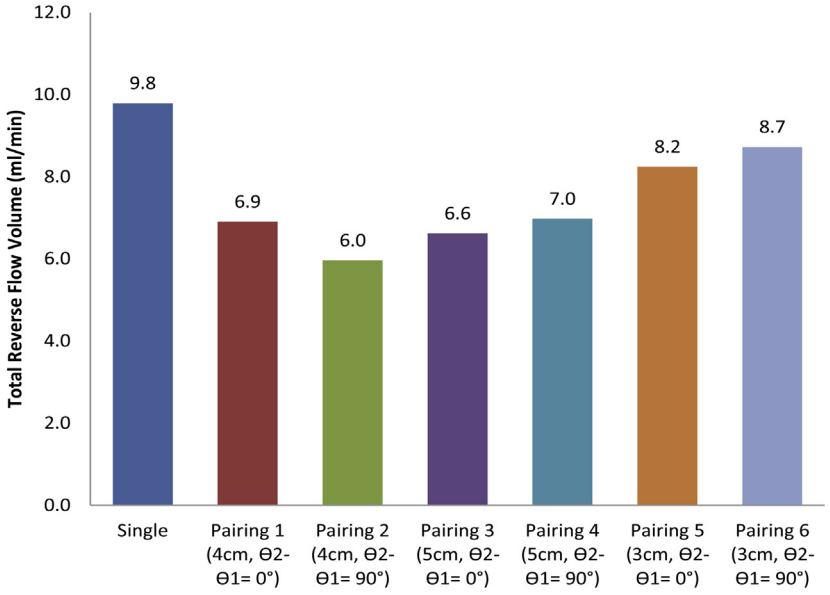


**Fig 5.** The total reverse flow volume of all the valve-pairing configurations tested in the current study.

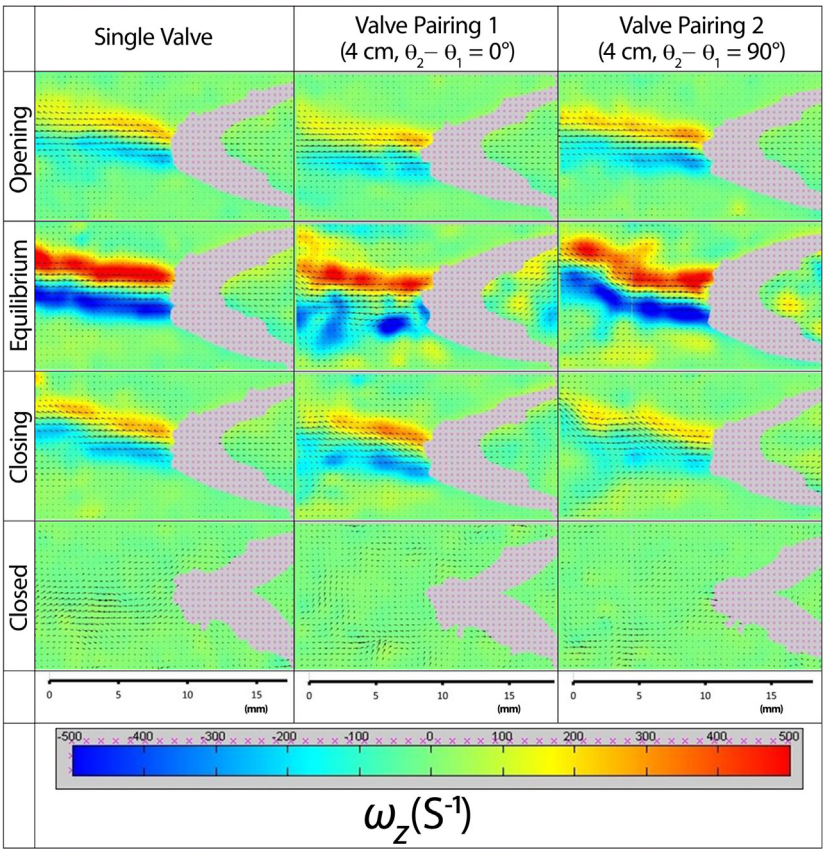


**Fig 6.** Velocity vector and vorticity maps of the valve cycle at the center plane of the valve region for different valve configurations.

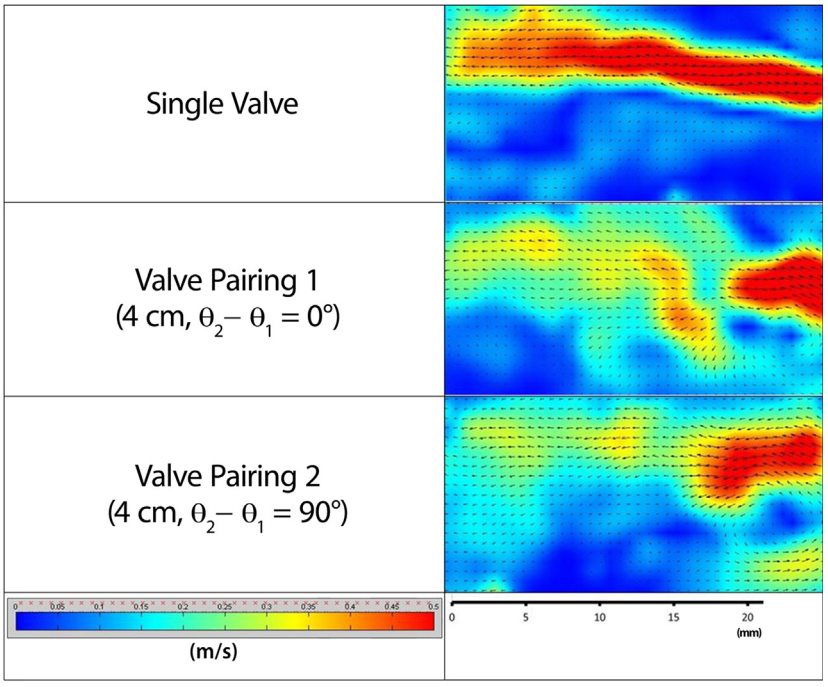


**Fig 7.** Velocity vector and velocity magnitude maps of the equilibrium phase for different configurations at the center plane of the downstream region. The *right edge* of the image is at 0.8 d downstream of the valve exit.

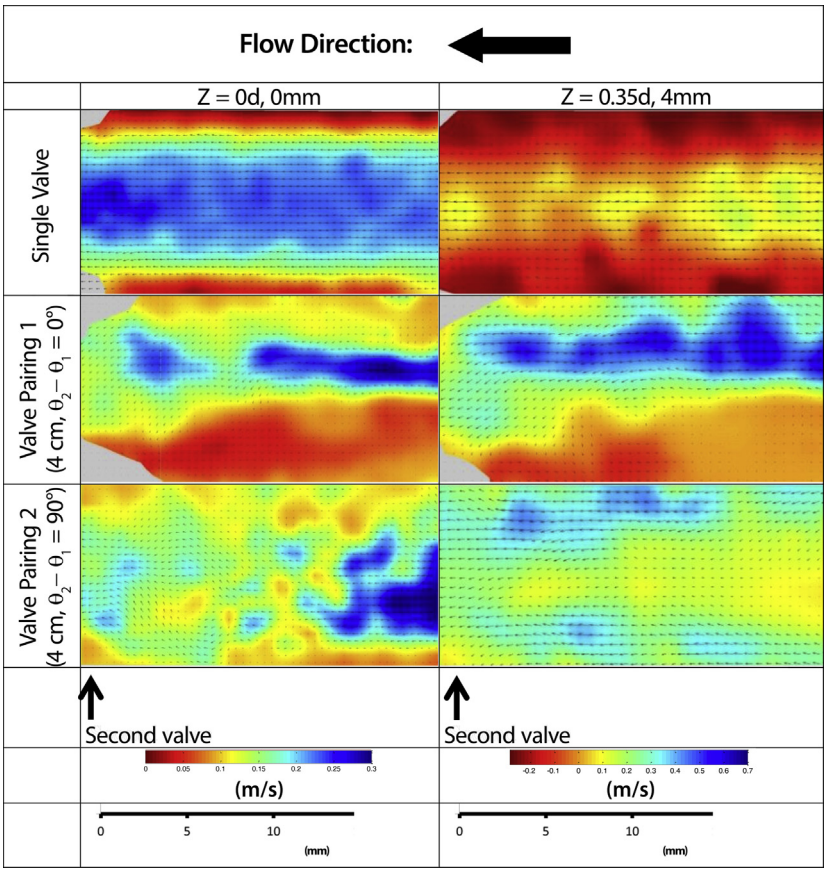


**Fig 8.** Velocity vector and the maps of the *u* component of the velocity of the equilibrium phase for valve pairing 1, 2, and single-valve case at center plane (Z = 0 mm) and edge plane (Z = 4 mm) in between two valves. The first valve (located upstream/distal side) is on the *right side* of the images, while the second valve (located downstream/proximal side) is located at the *left edge* as indicated by the *arrows*. Flow reversal was observed at valve pairing 1 and 2 and shown as *red color*.

fluid shear distributions were similar to the vorticity distributions. At the outer region, the strength of fluid shear becomes gradually weaker than the center plane. At Z = 0.35 d (4 mm), the fluid shear was significantly weaker and resulted in a smaller region of strong fluid shear. For the 0° configurations (pairing 1, 3, and 5), the jet stream direction was similar at different Z, with the difference in the strength and the width of the jet stream decreased with increase in Z. For the 90° configurations (valve pairing 2, 4, and 6), however, the jet stream had a larger turning angle toward the tube wall. The fluid shear was weaker, and the jet stream region shrank in width. The fluid shear was lower at Z = 0.35 d (4 mm), similar to the single-valve case.

Fig 11 shows the velocity integral along the x locations at different regions of a single valve and valve pairing 1 and 2. With the exception of the upstream region of the single valve in Fig 11, *a*, where the flow is the classical 2D Poiseuille flow, all other flow regions show a significant change in the velocity integrals. This implies that mass is not conserved in the X and Y direction and there must, therefore, be flow in the Z direction (ie, 3D flow). In all three regions, the variation in velocity integral is significantly larger for the valve pairing 1 and 2 than the single-valve case, suggesting the existence of complicate 3D flow structures.

## DISCUSSION

**Effect of valve configuration.** At the valve region of the second valve, the 90° valve pairing configuration creates a more stable flow pattern and, therefore, has better flow regulating effect over the 0° valve pairing configuration. From the equilibrium phase in Fig 6, it can be seen that the valve pairing breaks the stable shear flow structure seen in the single-valve case. In valve pairing 1, the shear layer broke up into unstable rollers. A slight phase lag between the two valves motions' was observed during the experiment and is likely the cause of this unsteady flow structure. In valve pairing 2, the shear layer was more continuous, but an abrupt turn could be observed toward the tube wall. This suggests a complicated flow structure was present for valve pairing 2.

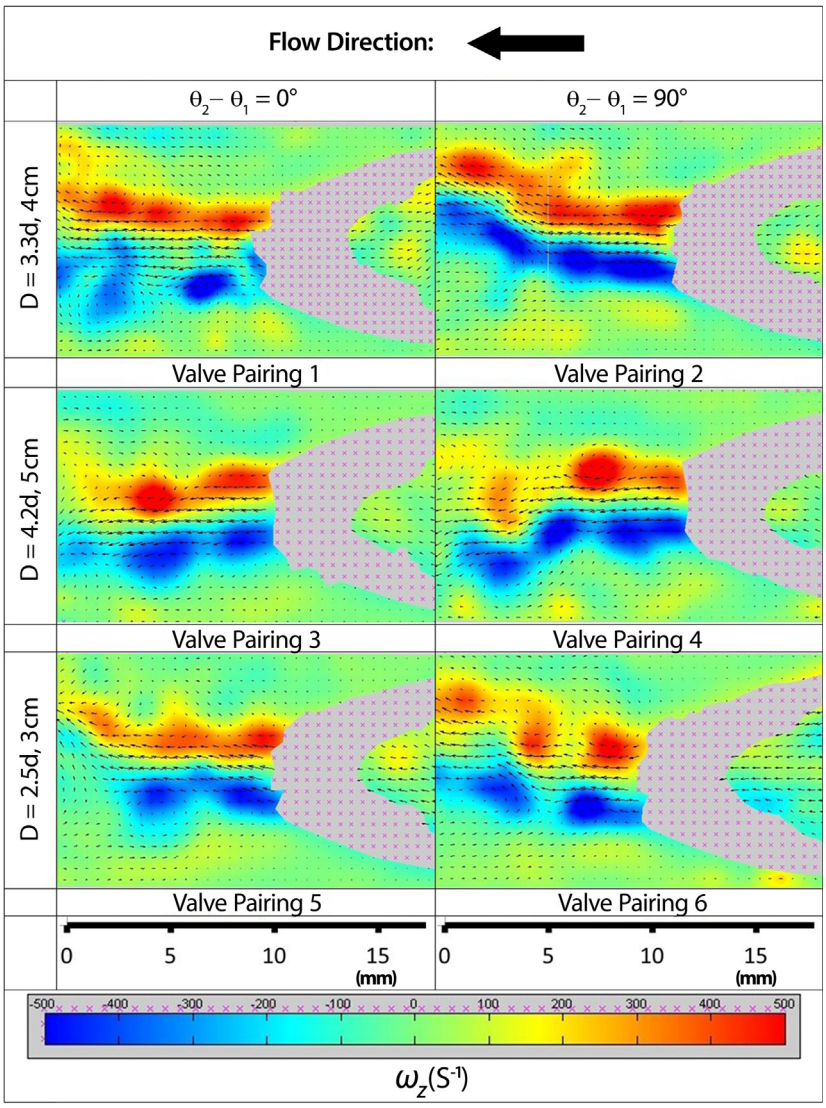


**Fig 9.** Velocity vector and the maps of vorticity of the equilibrium for different configurations at different separating distances in the valve region.

At the downstream region of the second valve, the exit jet flow mixed with the ambient flow quicker for valve pairing 1 and 2 than the single-valve case. Fig 7 shows that the jet flow spread out for both valve pairing 1 and 2 around 1.2 to 1.5 d, but in the single-valve case, the jet flow was maintained at least 2.8 d downstream of the valve exit. The fast decay of the jet velocity suggests more transfer of momentum in the out-of-plane direction and, therefore, mixing with the ambient flow.

At upstream region of the second valve, the pairing configuration significantly altered the flow structure between the valves, and the 90° configuration (valve pairing 2) has a lower risk of thrombosis over the 0° configuration (valve pairing 1) in between the valves. This is because the reverse flow region is eliminated in valve pairing 2. As shown in Fig 8, the flow patterns were similar for different Z locations for valve pairing 1, and the turning of the flow created a reversed flow region at the bottom half of the tube. On the other hand, the flows of valve pairing 2 (Fig 8) were different between Z planes. No reversed flow region like valve pairing 1 was observed for this case. All these observations suggest a complicated flow structure was formed in between the two valves for this valve configuration.

From the above observations, the 90° valve pairing configuration (valve pairing 2) provides a more stable flow pattern, creates less stagnant zones, and enhances mixing than a single valve. The blood is, therefore, transported more efficiently through the valves with less chance to stay in the dead zones of the tube. Lurie and Kistner[11] suggested that the orthogonal valve pairing configuration is preferred in nature because it creates the helical 3D flow

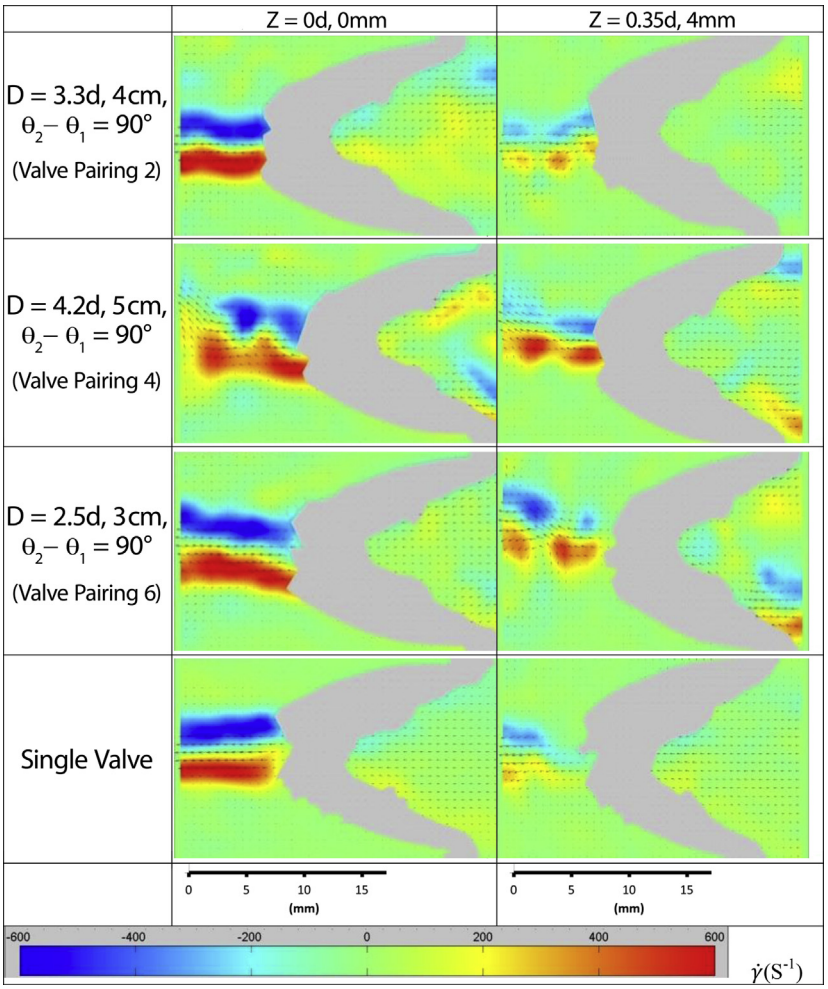


**Fig 10.** Velocity vector and the maps of the fluid shear of the equilibrium phase for valve pairing 2, 4, and 6 in the valve region.

pattern that increases the efficiency of the venous return flow. The current work is in agreement with their hypothesis.

**Effect of valve separating distance.** An optimum separation distance to minimize reverse flow existed only for the 90° valve pairing. The hemodynamics performances show that the total reverse flow volume is at minimum for valve pairing 2. The trends between the 0° configurations (valve pairing 1, 3, and 5) and the 90° configurations (valve pairing 2, 4, and 6) are different, and only in the 90° configurations the total reverse flow volume increased when the valves were too close (D = 2.5 d, 3 cm) and then increased again as the valves got further away (D = 4.2 d, 5 cm). Based on the video recordings of the valves, the valves' motions were observed to be slightly out of sync. Therefore, the valve coupling effect can cause a phase lag between the motions of the two valves. The incoherent motions may affect the sealing effect of the two valves and may be related to the valve separation distance. This is in agreement with the findings reported by Lurie and Kistner[11] that the distance between the two venous valves is about 4 cm. The fact that a minimum value of total reverse flow volume exists only in the 90° configurations is a subject worthy of further study.

The coupling effect of the valve pairing can last longer in the downstream tube, but the effect fades with longer separation distance. In the range tested in this work (D = 2.5-4.2 d), the flow around the downstream valves were all altered by the upstream valves, suggesting that the coupling effect extends beyond four times the tube diameter. With shorter separation distance, the coupling effect was stronger and the flow patterns between the 0° and 90° configurations were more distinct. On the other hand for D = 4.2 d in Fig 9, the flow patterns between valve pairing 3 and 4 were more similar at the center region. This is because the effect of the different valve pairing configurations was damped out as the distance increased.

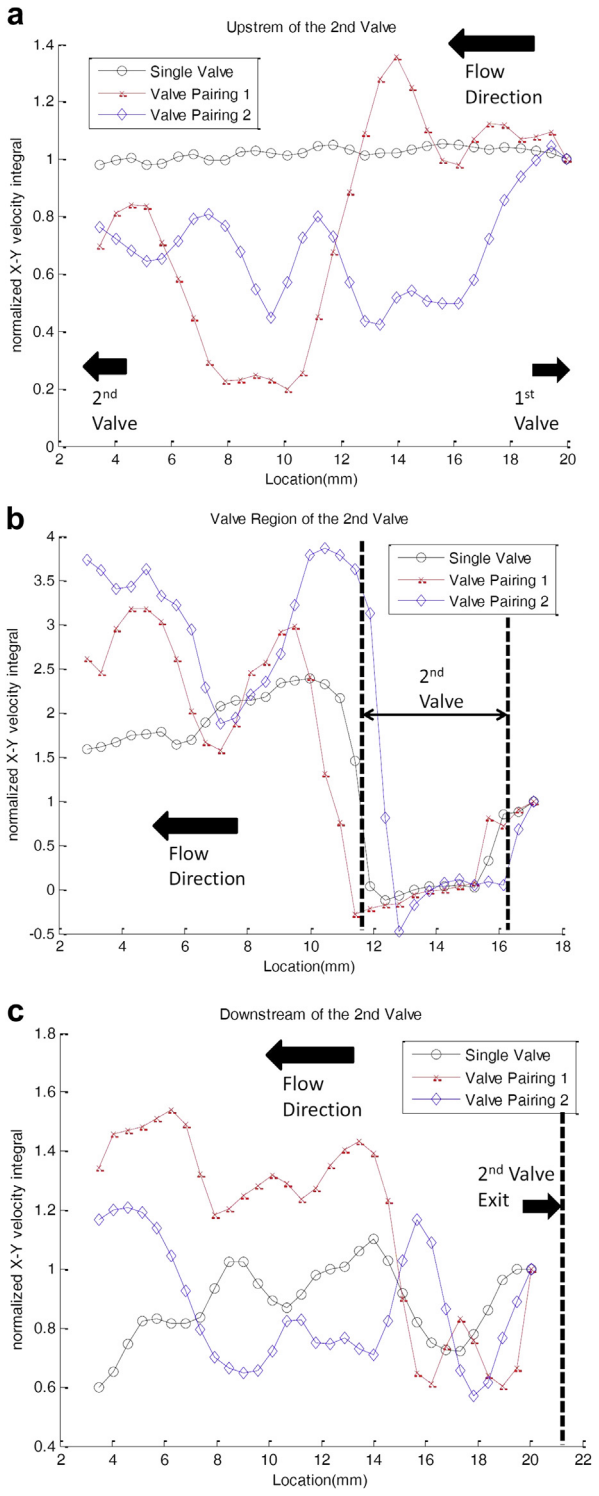


**Fig 11.** Variations of the velocity integral of the X and Y components across the tube along the X direction of different valve configurations at **(a)** upstream, **(b)** valve, and **(c)** downstream region. The momentum sum is normalized by values at the right end (upstream location of each region).

Fig 10 shows that the flow at the outer region of the tube was slower, and the jet stream width was also smaller than that at the center region. This is expected since the opening of the valve decreases at the edge. For the 90° configurations (valve pairing 2, 4, and 6), the flows were altered more at the edge. The jet stream turning angle was larger and started earlier than the center region. This variation in Z location also implies the flow has a likely 3D structure. The flow structure at the edge is likely beneficial to the venous flow because it reduces the stagnant region around the tube wall which may decrease the risk of thrombosis.

**Limitations of the study.** There are three main limitations of the current work. First, although the bioprosthetic valves mimic some aspects of the native bicuspid valves, there are still significant differences. The lack of sinus pocket for the bioprosthetic valves may change the flow significantly since the sinus may play a significant role in flow regulation.[5] Since this is a comparative study where both valves did not have a sinus, it is likely that the lack of sinus does not change the major conclusions of this study. Second, the use of solid glass tube does not represent the venous wall compliance. It is well known that the veins are compliant and can deform significantly. A solid glass tube may create a different wall shear stress distribution on the tube and alters the flow accordingly. This is not a significant limitation since the stress distribution has a long-term effect and may be less important to the flow patterns.

Third, the use of a 2D velocimetry technique does not allow direct measurement of the 3D flow field. As shown in the Results section, the flow field around the valves is 3D and significantly different from the single-valve case. A study using a full 3D velocimetry technique is necessary to understand the complex coupling effect of the valve and to reveal the helical nature of the flow pattern.

## CONCLUSIONS

In summary, complex flow patterns can be created with two valves pairing in different orientations. The 90° valve pairing configuration creates a stable flow pattern that can reduce the flow stasis region (ie, increase shear stress) and increase the efficiency (less reverse flow) of the valves. The 3D flow pattern also increases the mixing of blood. The distance between the valves affects the flow created by the two-valve pairing, and the separation distance affects the hemodynamic efficiency of the valve pairing.

The authors acknowledge the excellent technical expertise of Dr Chad Johnson and Mrs. Martha Spincer.

## AUTHOR CONTRIBUTIONS

Conception and design: WT, HC, ZB, JK, SC, DD, GK
Analysis and interpretation: WT, HC, ZB
Data collection: WT, HC, ZB
Writing the article: WT

Critical revision of the article: WT, HC, ZB, JK, SC, DD, GK
Final approval of the article: WT, HC, ZB, JK, SC, DD, GK
Statistical analysis: WT, HC, ZB
Obtained funding: JK, SC, GK
Overall responsibility: WT

## REFERENCES

1. Recek C. The venous reflux. Angiology 2004;55:541-8.
2. Bergan JJ, Schmid-Schönbein GW, Coleridge Smith PD, Nicolaides AN, Boisseau MR, Eklof B. Chronic venous disease. Minerva Cardioangiol 2007;55:459-76.
3. Karino T, Motomiya M. Flow through a venous valve and its implication for thrombus formation. Thromb Res 1984;36:245-57.
4. Lurie F, Kistner RL, Eklof B. The mechanism of venous valve closure in normal physiologic conditions. J Vasc Surg 2002;35:713-7.
5. Lurie F, Kistner RL, Eklof B, Kessler D. Mechanism of venous valve closure and role of the valve in circulation: a new concept. J Vasc Surg 2003;38:955-61.
6. Nam KH, Yeom E, Ha H, Lee SJ. Velocity field measurements of valvular blood flow in a human superficial vein using high-frequency ultrasound speckle image velocimetry. Int J Cardiovasc Imaging 2012;28:69-77.
7. Bergan JJ. The vein book. Elsevier Academic Press: Amsterdam; 2007.
8. Schweighofer G, Mühlberger D, Brenner E. The anatomy of the small saphenous vein: fascial and neural relations, saphenofemoral junction, and valves. J Vasc Surg 2010;51:982-9.
9. Tasch C, Brenner E. The ostial valve of the great saphenous vein. Phlebology 2012;27:179-83.
10. Mühlberger D, Morandini L, Brenner E. Venous valves and major superficial tributary veins near the saphenofemoral junction. J Vasc Surg 2009;49:1562-9.
11. Lurie F, Kistner RL. The relative position of paired valves at venous junctions suggests their role in modulating three-dimensional flow pattern in veins. Eur J Vasc Endovasc Surg 2012;44:337-40.
12. Lurie F, Kistner RL. On the existence of helical flow in veins of the lower extremities. J Vasc Surg Venous Lymphat Disord 2013;1:134-8.
13. Mohiaddin RH, Yang GZ, Kilner PJ. Visualization of flow by vector analysis of multidirectional cine MR velocity mapping. J Comput Assist Tomogr 1994;18:383-92.
14. Kilner PJ, Yang GZ, Mohiaddin RH, Firmin DN, Longmore DB. Helical and retrograde secondary flow patterns in the aortic arch studied by three-directional magnetic resonance velocity mapping. Circulation 1993;88(5 Pt 1):2235-47.
15. Stonebridge PA, Brophy CM. Spiral laminar flow in arteries? Lancet 1991;338:1360-1.
16. Caro CG, Doorly DJ, Tarnawski M, Scott KT, Long Q, Dumoulin CL. Nonplanar curvature and branching of arteries and nonplanar-type flow. Proc R Soc Lond A 1996;452:185-97.
17. Morbiducci U, Ponzini R, Rizzo G, Cadioli M, Esposito A, De Cobelli F, et al. In vivo quantification of helical blood flow in human aorta by time-resolved three-dimensional cine phase contrast magnetic resonance imaging. Ann Biomed Eng 2009;37:516-31.
18. Morbiducci U, Ponzini R, Rizzo G, Cadioli M, Esposito A, Montevecchi FM, et al. Mechanistic insight into the physiological relevance of helical blood flow in the human aorta: an in vivo study. Biomech Model Mechanobiol 2011;10:339-55.
19. Pavcnik D, Uchida B, Kaufman J, Hinds M, Keller FS, Rösch J. Percutaneous management of chronic deep venous reflux: review of experimental work and early clinical experience with bioprosthetic valve. Vasc Med 2008;13:75-84.
20. Raffel M, Willert CE, Wereley ST, Kompenhans J. Particle image velocimetry: a practical guide. Springer Berlin Heidelberg: New York; 2007.
21. Westerweel J, Scarano F. Universal outlier detection for PIV data. Exp Fluids 2005;39:1096-100.

Submitted Jun 27, 2013; accepted Sep 22, 2013.